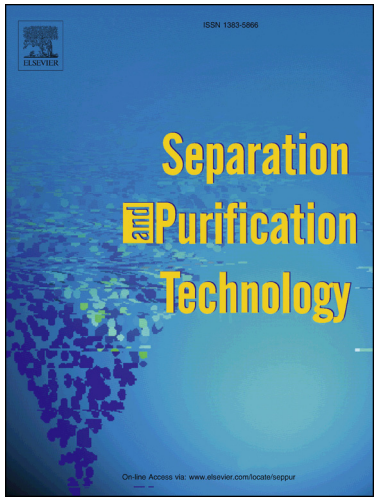

A Model of Backpulse and Backblow Cleaning of Nanofiber Filter loaded with Nano-aerosols

Wallace Woon-Fong Leung, Curie Wing-Yi Hau

PII: S1383-5866(16)30622-0
DOI: http://dx.doi.org/10.1016/j.seppur.2016.06.007
Reference: SEPPUR 13063

To appear in: *Separation and Purification Technology*

Received Date: 14 March 2016
Accepted Date: 2 June 2016

Please cite this article as: W.W-F. Leung, C.W-Y. Hau, A Model of Backpulse and Backblow Cleaning of Nanofiber Filter loaded with Nano-aerosols, *Separation and Purification Technology* (2016), doi: http://dx.doi.org/10.1016/j.seppur.2016.06.007

A Model of Backpulse and Backblow Cleaning of Nanofiber Filter loaded with Nano-aerosols

Wallace Woon-Fong Leung* and Curie Wing-Yi Hau

Mechanical Engineering

The Hong Kong Polytechnic University,

Hung Hom, Hong Kong

*Corresponding author

ABSTRACT

A two-parameter model has been developed to interpret the pressure excursion during cleaning of a nanofiber filter preloaded with nano-aerosols. The model can well predict the three stages of cleaning – an initial rapid cake discharge phase, a transition and a final phase, both of which are related to cleaning aerosols trapped in the filter. One of the two parameters affects the residual pressure drop while the other parameter affects the cake discharge. The filter cleaning test data based on variations from the five operating and geometric parameters have been explained by the new model – the backpulse, backblow, and combined mode; pulse duration; applied over-pressure; diameter of nanofiber in filter; and the filter thickness. Furthermore the model can project the residual pressure, which provides an indication of residual aerosols trapped in the filter, using individual or combination of these operating and geometric parameters.

Keywords: Cleaning Model, Loaded Nanofiber filter, Nano-aerosols, Backpulse, Backblow; Residual Pressure drop; Cake; Residual aerosols

1. BACKGROUND

Nano-aerosols are airborne aerosols typically less than 100 nm (which is the same as ISO/DIS 19430(en) standard on nano-particles). They can be pollutants that lead to chronic diseases or viruses that are harmful to our health. Filters made from nanofibers with diameters 100-300 nm can effectively capture these nano-aerosols. Over time in operation, the filter is loaded with aerosols and the pressure drop across the filter can be significant. At that point the filter needs to be replaced or requires cleaning. While there are numerous studies concerning cleaning of conventional bag-house filters [1-12], there is limited publication on cleaning of loaded nanofiber filter.

Hau and Leung [13] have investigated experimentally backpulse, backblow and their combined mode on cleaning of nanofiber filter preloaded with nano-aerosols. Three stages in pressure changes have been observed in cleaning of a nanofibrous filter preloaded with nano-aerosols. This can be referenced to Fig. 1 wherein all the pressure drops during cleaning of the loaded filter has been normalized $\Delta P'$ after the pressure drop of a clean filter ΔP_f has been subtracted, i.e. $\Delta P' = \Delta P - \Delta P_f$.

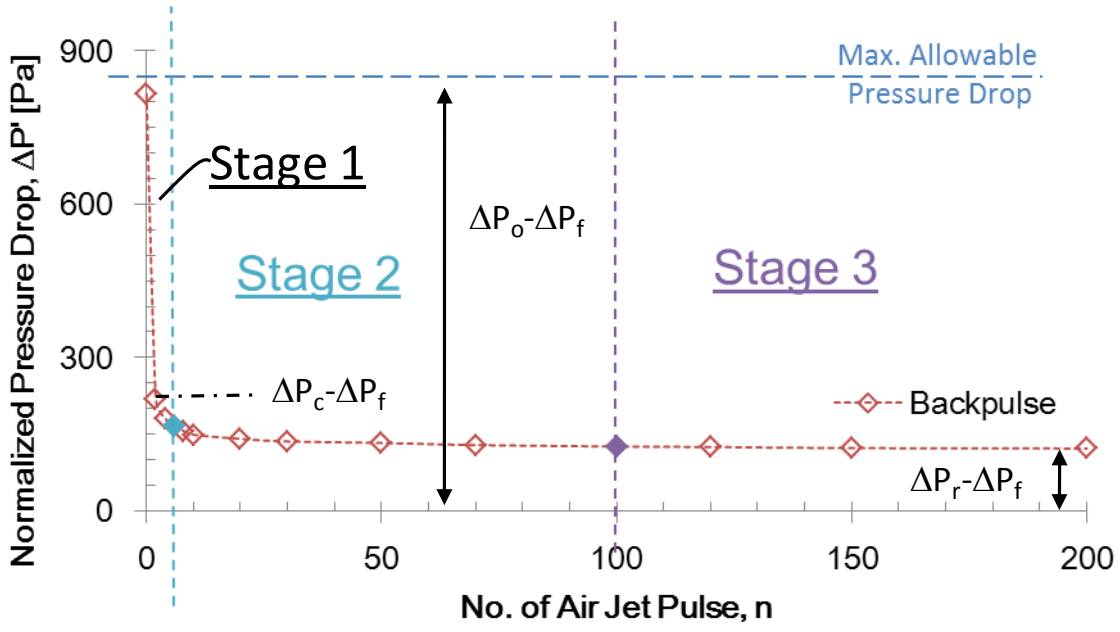

Fig. 1 – Typical three stages in cleaning of a nanofibrous filter

The three stages for backpulse have the characteristics as follows:

The first stage corresponds to removal of the cake by the airflow. Once the cake is removed, the aerosols trapped in the nanofiber filter can be blown off initially in greater amount (second stage) to be followed with diminishing amount at the third or final stage.

Concurrently, the aerosols can be re-deposited further upstream of the filter resulting in lesser amount being removed from the filter. Accordingly, these three stages can be delineated [13] according to

Stage 1: $$\left|\frac{d\left(\Delta P'\right)}{dn}\right| \geq 30 \quad (1)$$

Stage 2: $$0.1 < \left|\frac{d\left(\Delta P'\right)}{dn}\right| < 30 \quad (2)$$

Stage 3: $$\left|\frac{d\left(\Delta P'\right)}{dn}\right| \leq 0.1 \quad (3)$$

where $\Delta P'$ is the normalized pressure drop
n is the number of jet pulses.

On the other hand, for backblow, the three stages are defined by:

Stage 1: $$\left|\frac{d\left(\Delta P'\right)}{dt}\right| \geq 30 \quad (4)$$

Stage 2: $$0.1 < \left|\frac{d\left(\Delta P'\right)}{dt}\right| < 30 \quad (5)$$

Stage 3: $$\left|\frac{d\left(\Delta P'\right)}{dt}\right| \leq 0.1 \quad (6)$$

where dt is the backblow duration.

Closer examination of these three stages reveals some subtle yet interesting aspects.

Stage 1 - Cake removal:

The cleaning of the loaded nanofibrous filter involves first blowing out the cake if a cake layer has already been deposited on the filter surface. In this process, part of the deposited aerosols can be redistributed in the nanofiber filter, in which the aerosols deposited downstream of the filter may be detached and re-deposited at the upstream end of the filter, and even on the back-side of the cake. Once the cake is blown off from the filter, there is a chance that these detached aerosols can leave the filter with the airflow. This is represented by the pressure drop from the maximum allowable pressure ΔP_o down to ΔP_c.

Stage 2 - Initial depth-filter cleaning:

Upon the cake being removed, the airflow from backpulse or backblow can further remove the aerosols attached to the nanofibers as well as aerosols forming agglomerates or dendrite structures in the filter. However, the nano-aerosols can get re-

trapped at the upstream end of the filter by diffusion and interception. Thus, both detachment and recapture can take place at different locations of the filter. In this stage, the detachment rate is larger than the recapture rate as pressure drop can be decreased with further backpulse or backblow.

Stage 3 - Final depth-filter cleaning:

In this stage, airflow from backpulse or backblow removes the aerosols attached to the nanofibers as well as to other aerosols forming agglomerates or dendrite structures. Again, these aerosols can deposit back at the upstream end of the filter. Ultimately an equilibrium would be reached in which aerosols removal rate is more or less balanced by the re-deposition rate in which there is no further change in aerosols (and pressure drop) in the filter with further backpulse or backblow. Another possible scenario is that the remaining aerosols that are attached has adhesion force (due to large contact surface area and dead pores) that are much greater than the existing driving force from backpulse or backblow unless much higher driving force is required for which there is potential risk of damaging the nanofibers in the filter. Both scenarios are consistent with virtually nil-to-little pressure drop change being observed across the filter with further backpulse, or backblow, in this final stage. This residual pressure drop is designated Δp_r.

While previous work [13] has qualitatively delineated the general behavior of jet cleaning of a loaded filter, including various operating modes (such as backpulse, backblow and combined mode; pulse duration; and applied over-pressure on driving the air jet.) it would be useful to quantify these effects by a model and to determine using the model whether combined operating cleaning modes can further achieve even lower residual aerosols in the filter. All the aforementioned parameters concern the positive cleaning aspects, there are factors that negatively impact cleaning, such as increase in adhesion of the aerosol to the nanofiber filter and also increase in filter thickness that further increases recapture of the airborne aerosols. These additional negative aspects on filter cleaning need also to be accounted for by the model.

Based on the above unmet needs, a new model will be developed herein to explain and predict the behavior of the pressure drop curve during jet cleaning by backpulse, backblow and the combined mode. The model will grossly quantify the effect of backpulse, backblow and their combined mode; pulse durations; applied over-pressure; adhesion of aerosols from filters with nanofibers of different diameters; and also increase of recapture of detached aerosols from increasing filter thickness. The model should also predict the impact from individual parameter, or combination of parameters. Further experiments will also be carried out to produce test results on cleaning behavior for filters with different nanofiber diameters and different thicknesses for use by the model.

2. MODEL

An empirical model that uses two parameters *a* and *b*, is used to describe the cleaning behavior due to backpulse, backblow and their combination:

$$\frac{\Delta P - \Delta P_f}{\Delta P_o - \Delta P_f} = \exp(-a\left[\frac{n}{N}\right]^b) \quad (7)$$

where ΔP is the pressure drop of the filter during cleaning, ΔP_f is the pressure drop of the clean filter without aerosol deposit, and ΔP_o is the maximum pressure that the filter can reach during aerosol loading. *N* is the total number of backpulses and *n* is the number of backpulses from start of cleaning. Therefore, the ratio $n/N \leq 1$ represents the cleaning effort.

Parameter *a* is a function of the ratio of the detachment-to-adhesion forces of aerosol to the nanofibers. The attachment force of the aerosols to the nanofibers is largely due to Van der Waal's force. Further, parameter *a* is also a function of re-capturing of nano-aerosols by the nanofiber filter. For this aspect, increasing fiber diameter, increasing face velocity, reducing filter thickness, and reducing nanofiber volume fraction, etc. all contribute to decreasing the recapture of detached airborne nano-aerosols. Of interest is that increasing face velocity, which increases the shear to detach aerosols from the nanofibers, further reduces the chance of aerosol re-capture by the nanofiber filter, especially by diffusion capture as it takes time for the diffusion process to be effective. However, the velocity cannot be too excessive so as to induce high shear that can cause damage to nanofibers in the filter.

The parameter *b* is largely related to the adhesion force (interfacial force) of the cake to the filter surface to the detachment force on the cake. As will be shown, the detachment of the cake depends largely on the parameter *b* and to some smaller extent also on *a* as well.

As can be seen, the problem on cleaning of the filter is rather complex. Unlike the conventional baghouse filter, this is also complicated by the fact that the there is a maximum velocity that one cannot exceed to avoid nanofiber damage, and aerosols that have been detached from the fibers can be recaptured readily by the nanofiber filter downstream of the flow. These two aspects are quite a departure from the conventional baghouse filter.

3. EXPERIMENTS

The details of the experiment on the fabricating of nanofibers from needless electrospinning and the experimental set-up on generating nano-aerosols from sodium chloride solution have been discussed earlier [13]. As schematically represented by Fig. 2a, nano-aerosols between 40-300 nm in a polydispersed range (nominally

60%<100nm, and 90%<160nm) were used to challenge the test nanofiber filter with fiber diameter 120-280nm. After the pressure drop has reached the maximum ΔP_o (typically about 800Pa), the filter undergoes cleaning by backpulse, backblow, or backpulse-and-backblow as shown in Fig. 2b. The schematics for these cleaning mechanisms are depicted in Figs. 3a-c, respectively.

The experimental results reported [13] will be used for verifying the model. Additional experiments have also been conducted to increase the adhesion force on the aerosols especially to test out the third stage on residual pressure as a result of residual aerosols left in the filter after cleaning. To that end, three different filters have been selected in the tests corresponding to nanofibers with average diameters 120, 180 and 280nm. In some cases, two to three filters of the same fiber diameter but different filter thicknesses were tested.

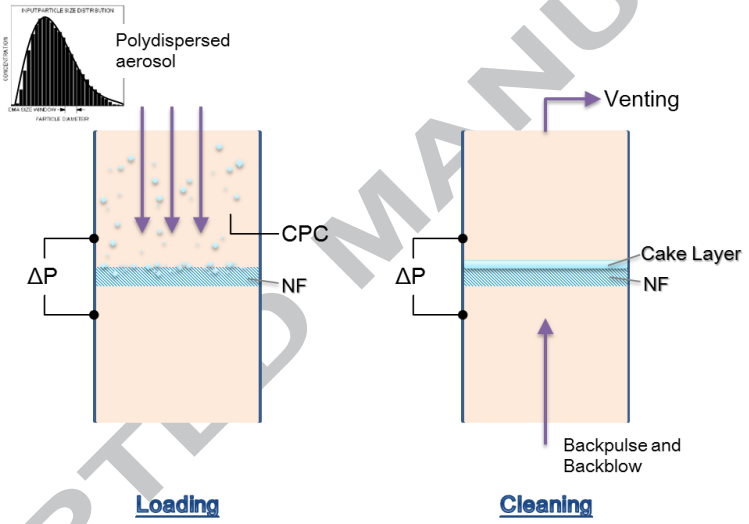

Fig. 2 - Experimental setup of test column during consecutively (a) loading and (b) cleaning (backpulse, backblow, and combined backpulse-and-backblow).

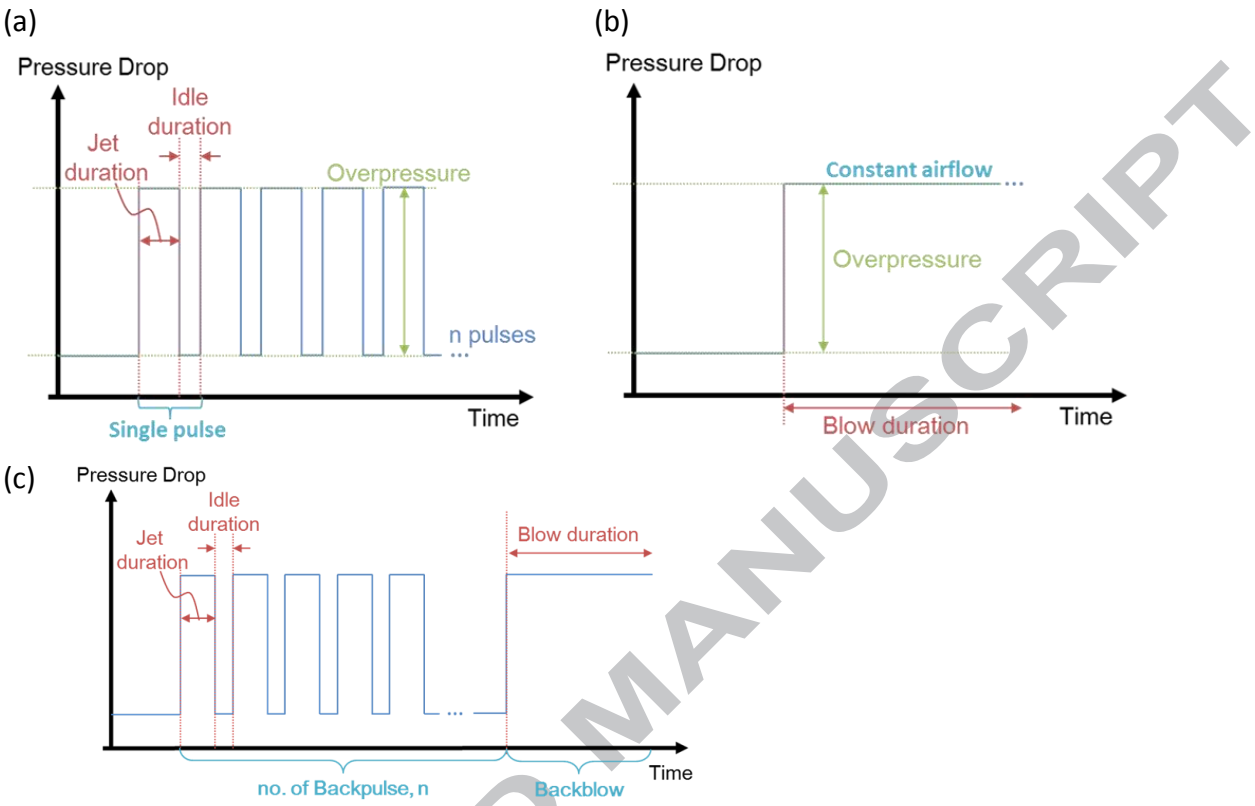

Fig. 3 - The work logics of (a) backpulse, (b) backblow and (c) combined backpulse-followed-by-backblow

4. RESULTS AND DISCUSSIONS

4.1 Effect of applied pressure on cleaning

Fig. 4a shows three experimental cleaning trends that have been normalized in both abscissa and ordinate scale according to the labels. These three trends correspond to, respectively, to 3, 4, and 6.5 bar over-pressure. The continuous curves are the model prediction from Eq. 1 that best match to the experimental data. The values of the two parameters *a* and *b* are shown in Fig. 4a.

In general, matching between the experimental results and the model prediction can be done well for both the first stage when cake is blown out from the filter as well as for the third stage when cleaning equilibrium has been reached (no additional aerosols removal or removal rate of aerosols equals recapture rate). The second stage, which is also the

transition stage of initial depth filter clean-out, is hard to predict despite 6.5 bar cleaning is reasonably accurate, while 3 and 4 bars seem to under-shoot.

In this part, only the driving force has been increased keeping all other parameters constant. This should yield a higher velocity jet (which may be proportional to $\Delta P^{1/2}$.) assuming the dynamic pressure $\frac{1}{2}\rho V^2$ is related to the over-pressure. Higher jet velocity results in increasing detachment force and reducing also the recapture of the loosened aerosols downstream of the filter. The residual ratio r can be defined as

$$r = \frac{\Delta P_r - \Delta P_f}{\Delta P_o - \Delta P_f} \tag{8}$$

The values of *a* are 1.1, 1.3 and 1.8 corresponding to 3, 4, and 6.5 bars overpressure, respectively. In fact, $a \propto \Delta p^{0.65}$. This means that increasing the overpressure has a non-linear effect on a. As stated, *a* depends largely on driving force to attachment Van der Waal force, the larger is the magnitude of *a* the better is the cleaning and lower is the value *r*.

Fig. 4b shows a plot of the normalized residual pressure r with the three values of r corresponding to the three values of over-pressures. The decreasing trend of r versus increasing *a* is evident. Also, from the model when $n/N \rightarrow 1$, $(n/N)^b \rightarrow 1$ irrespective of the value of b, thus, Eq. 1 can be simplified to

$$r = \frac{\Delta P_r - \Delta P_f}{\Delta P_o - \Delta P_f} \approx \exp(-a) \tag{9}$$

This gives *ln r = -a*, which is a straight line on a semi-log plot! This prediction line compares excellently with the three data on r vs. a in fig. 4b. Of interest is that if all the conditions are kept constant other than the over-pressure, it is possible to predict the necessary over-pressure required to meet a certain residual *r*. For example, when *r*=0.05, *a*=2.995 as calculated from Eq. 9. Using the relationship that $a \propto \Delta p^{0.65}$ with the base case *a*=1.8 when Δp*=6.5 bars,* if *a=2.998,* Δp needs to be 14.2 bar. This is too high for the nanofibers, not until after reinforcement and adhesive. In any event, this illustrates the point.

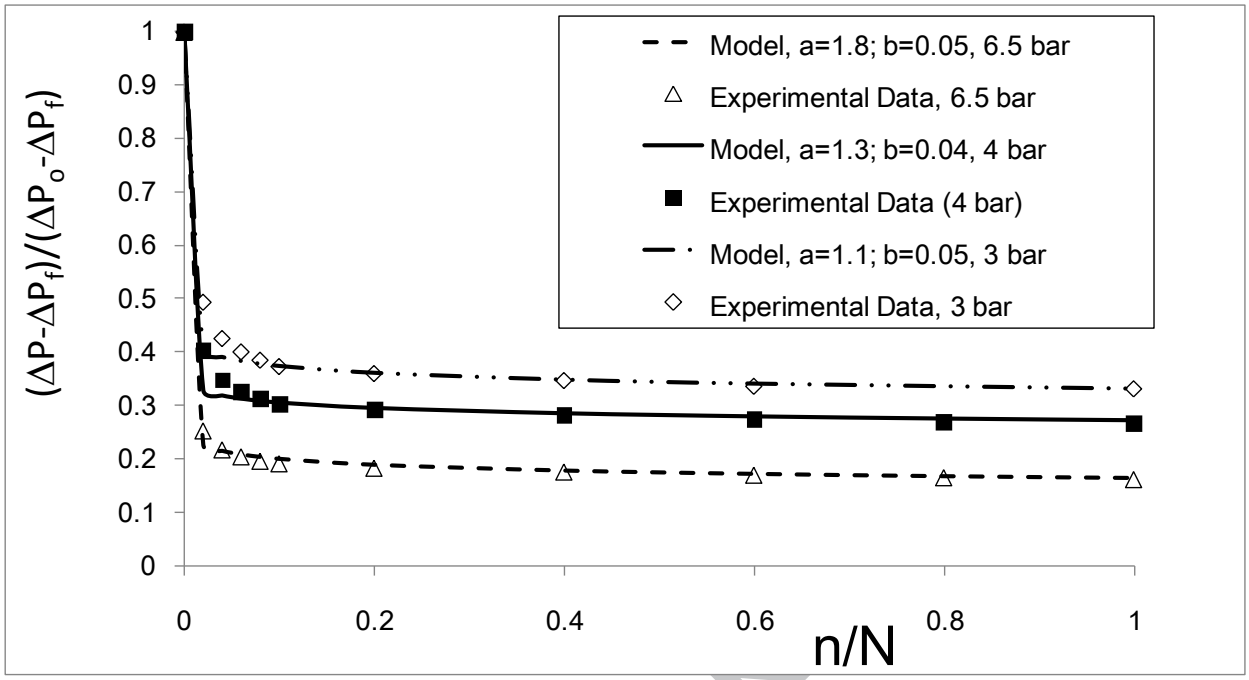

Fig. 4a – Comparing experiments and prediction from cleaning due to variation in applied over-pressure.

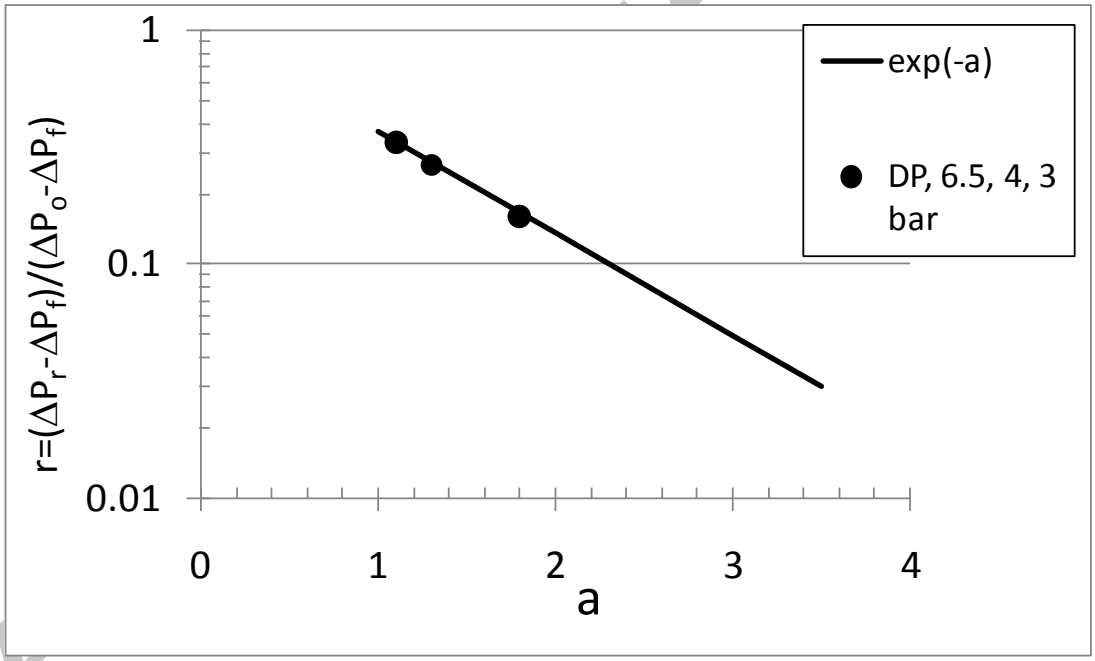

Fig. 4b - Residual plotted again a for over-pressures of 3, 4 and 6.5 bars.

4.2 Effect of Backpulse, backblow, and combined backpulse-backblow, and jet durations

4.2.1 Residual aerosols and residual pressure drop

Comparison of test results and model prediction for the effect of backpulse (BP), backblow (BB) and their combined mode is illustrated in Fig. 5. As can be seen, there may be large deviations between experiments and prediction for the second stage (tarnsition) to be followed by a short third and final stage reaching closely the residual pressure drop.

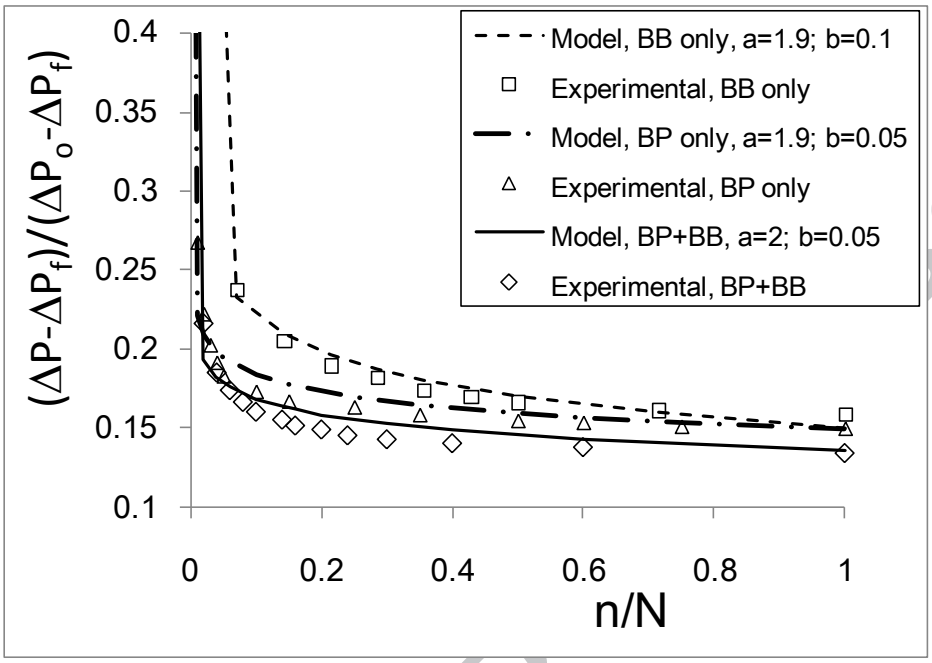

Fig. 5 – Matching model with experiments for backpulse, backblow and their combined mode.

The residual ratio r is plotted against *a* in Fig. 6 in a semi-log manner. Several observations are evident.

(1) All the data irrespective of operation - backpulse or backpulse and backblow, and pulse durations 0.1 - 0.5s, clearly lie closely on the r=exp(-a) line on the semi-log plot. This is in accord with the same behavior as the different over-pressures driving the backpulse and backblow in Fig. 4b.

(2) The lowest empty triangle in Fig. 6 for the combined backpulse and backblow mode is distinctly lower than the two empty triangles above, which are for backblow (higher between the two modes) and backpulse (lower between the two), respectively.

(3) The "empty squares" for the combined backpulse and backblow mode has larger *a*, thus lower *r*, compared to just backpulse alone (empty circles). This reiterates the fact that the combined mode offers more cleaning with backpulse loosening the aerosols and with backblow further blowing the loosened aerosols out of the filter.

(4) For both combined backpulse-and-backblow mode and backpulse only, lower *r* is a result of longer pulse durations. That is 0.5s pulse is better than 0.3s, which in turn is more favorable than 0.1s. This confirms that longer jet duration provides the jet with increasing momentum and mass for loosening and shearing the attached aerosols from the nanofibers.

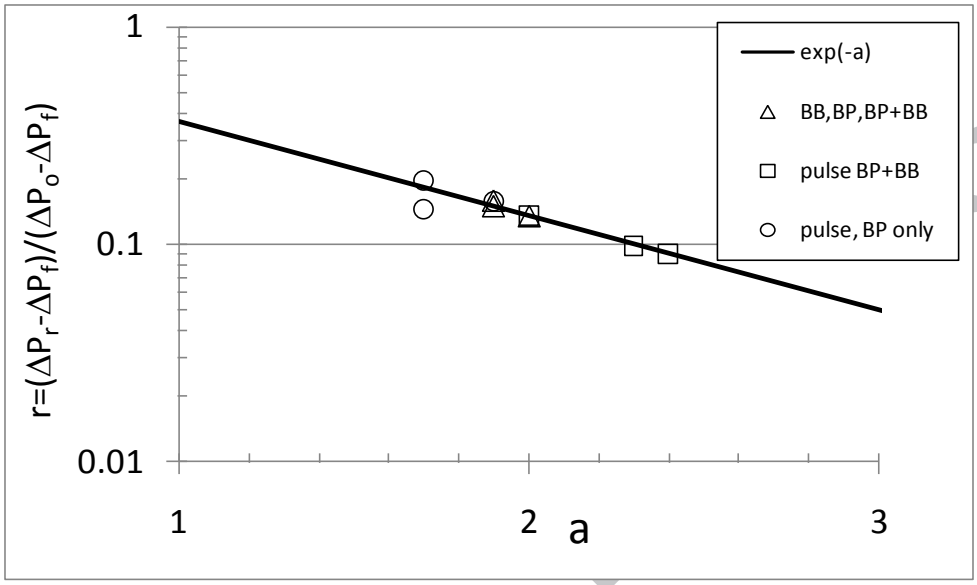

Fig. 6 – The residual pressure ratio *r* as a function of *a* for backpulse only with different durations 0.1, 0.3, and 0.5s, and their combined modes also with different durations 0.1, 0.3, and 0.5s.

4.2.2 Cake discharge

The prerequisite for cleaning the depth filter is to remove the cake deposited on the filter surface, which is the first stage of cleaning. This usually takes place in the first 10 pulses in most cases. With n_c=10 and N=500, this corresponds to n_c/N=0.02. The pressure drop starts dropping precipitously from ΔP_o down to ΔP_c. The change in pressure drop ΔP_o - ΔP_c represents the amount of cake being removed by the cleaning mechanism being considered. This can be compared to the maximum pressure drop possible if all the aerosols are removed with pressure drop reduced by a magnitude of, ΔP_o - ΔP_f. Thus, the ratio

$$\frac{\Delta P_o - \Delta P_c}{\Delta P_o - \Delta P_f}$$

represents the effectiveness of cake removal or the dimensionless pressure drop from cake discharge. Assuming it takes n_c pulses to effect the cake discharge and ΔP drops to ΔPc, Eq. 7 can be arranged as

$$\frac{\Delta P_o - \Delta P_c}{\Delta P_o - \Delta P_f} = 1 - \frac{\Delta P_c - \Delta P_f}{\Delta P_o - \Delta P_f} = 1 - \exp(-a\left[\frac{n_c}{N}\right]^b) \quad (10)$$

In Fig. 7, the dimensionless pressure drop from cake discharge as measured by the experiments (ordinate scale) is plotted against the analytical expression on the RHS of Eq. 10 (abscissa), which represents the driving force for cake discharge. The experiments covered backpulse and backblow, and different jet pulses duration. First, the measured cake discharge dimensionless pressure drop for all the test conditions agree reasonably well with the theoretical prediction (RHS of Eq. 10) as the data lie close to the 45-degree line. Second, backpulse-and-backblow is much more effective in discharging the cake than using either backpulse or backblow. Third, the duration of the pulses may not affect much on the cake discharge, i.e. longer and shorter pulses have similar effect.

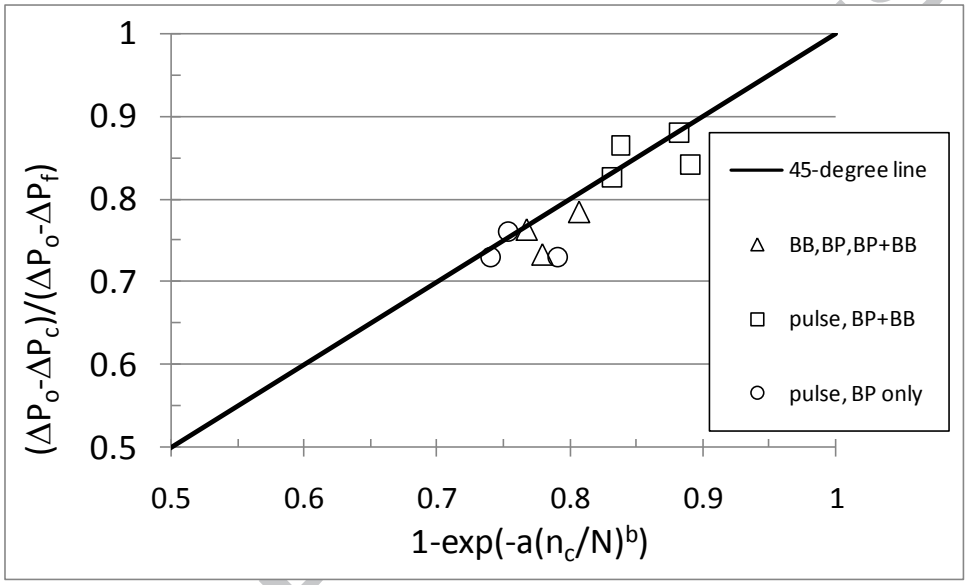

Fig. 7 – Cake discharge indication from experiments versus model prediction.

4.3 Effect of nanofiber diameter on jet cleaning

In the foregoing, the effect of driving force (jet magnitude, jet pulsation, etc.) on filter cleaning has been examined. It would also be useful to examine the opposite on effect of changing adhesion of the aerosols to the nanofibers which affects air jet cleaning of the filter. Experiments have been carried out along the same protocols [13] but with test filters of different average nanofiber diameters of 120, 180 and 280nm, respectively. The average pressure drop for these three filters under clean state before aerosol loading is between 26 and 30 Pa. The results are shown in Figs. 8a and 8b. The characteristics of three stages remain the same. The larger fiber diameter 280nm filter has less area per unit filter area or filter volume for the Van der Waal force to act on, the lower is the adhesion of aerosol to the nanofibers, thus the trapped aerosols can be removed more readily for the same detachment forces (inertial force from vibration of

the filter due to the jet pulses and shear force from the accompanied airflow) as compared to the case of 180nm, and progressively 120nm. As a result, the residual ratio reduces to the lowest value for 280nm, followed by 180nm, and lastly 120nm.
After matching with the experimental data, the parameters *a* and *b* were deduced by the model. The prediction from the model using these parameters are compared with the experimental data in Fig. 8a and also more clearly in the exploded view of Fig. 8b.

Further, *r* is plotted against *a* in Fig. 8c. As evident, the filters with different fiber diameters also agree excellently with the relationship, $r=\exp(-a)$. Given *a* is a function of detachment-to-adhesive forces, *a* is increased when the adhesion is reduced. Therefore, by increasing the fiber diameter from 120nm, 180nm, and finally 280nm, *r* is progressively reduced as seen in Fig. 8c!

The cake discharge behavior can be seen in Fig. 8d by plotting the dimensionless pressure drop from cake discharge $(\Delta P_o-\Delta P_c)/(\Delta P_o-\Delta P_f)$ against the modified driving force $1-\exp(-a[n_c/N]^b)$. It is clear that the 280nm nanofiber filter has the largest dimensionless pressure drop, followed by 180nm nanofiber filter, and lastly 120nm nanofiber filter. The magnitude of such pressure drop represents largely the removal of the cake (being the major flow resistance) and to some extent also loosened aerosols in the depth filter as blown out by the air jet along with the cake discharge. It is a reasonable conjecture that the attachment of the cake onto the 280nm filter surface is less compared to 180nm and further 120nm as the nanofiber area in contact with the cake is less. This characteristics should be evident by examining Fig. 8d on the modified driving force (i.e. abscissa scale) and the result (i.e. ordinate scale). Indeed, both abscissa and ordinate values for 280nm is greater than the corresponding values from 180nm, which in turn is greater than the corresponding values from 120nm.

4.4 Effect of filter thickness on jet cleaning

For the nanofiber filter with 280nm fiber diameter, three filters each with different thickness have been tested, see Table 1. The pressure drop before aerosols loading was measured as 16, 26 and 34Pa. Assuming Darcy flow, pressure drop varies with the filter thickness. Thus, the 26Pa filter has 1.6x the thickness of the 16Pa filter, while the 34Pa filter has 2.1x the thickness of the 16Pa filter. Increasing filter thickness also translates to increasing recapture of the loosened aerosols and thus lower *a* and concurrently higher *r*. This is seen in Table 1 and also in Fig. 8c.

Table 1 – Comparing 3 nanofiber filters with same fiber diameter but with different filter thickness

Filter (280nm dia.)	h / h(16Pa)	r	a	b
16 Pa	1	0.0369	3.3	0.0369
26 Pa	1.6x	0.0952	2.3	0.0952
34 Pa	2.1x	0.1041	2.3	0.1041

Fig. 8d also reveals that the cake discharge dimensionless pressure is higher for the thinner filter with ΔP_f=16Pa as compared to ΔP_f=26Pa, and also ΔP_f=34Pa. While cake discharge force for the 16Pa filter is distinctly higher as compared to the other two filters.

The foregoing experiments and interpretation using the model allow us to interpret the air jet cleaning behavior of nanofiber filter based on varying (1) the adhesion of the aerosols to the nanofibers of different diameters and (2) the adhesion of the cake onto the filter surface with different fiber diameters.

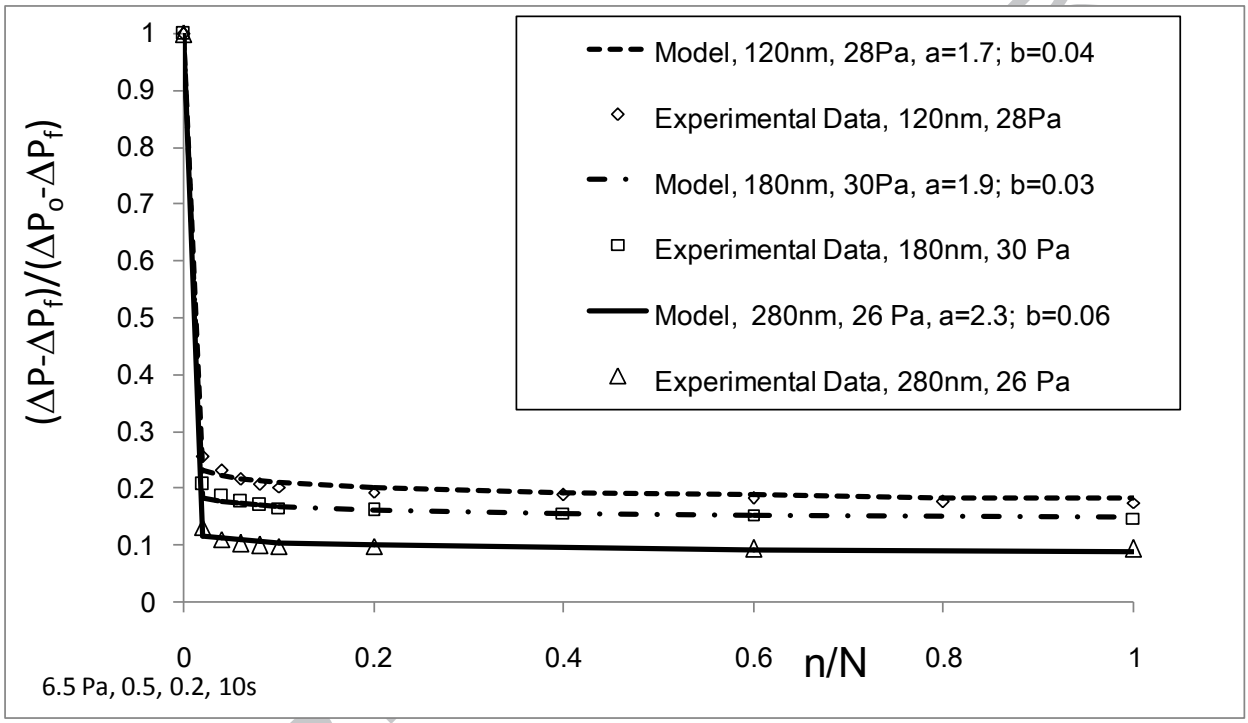

Fig. 8a - Pressure excursion across the filter during cleaning for the 3 filters with fiber diameter respectively 120, 180 and 280nm.

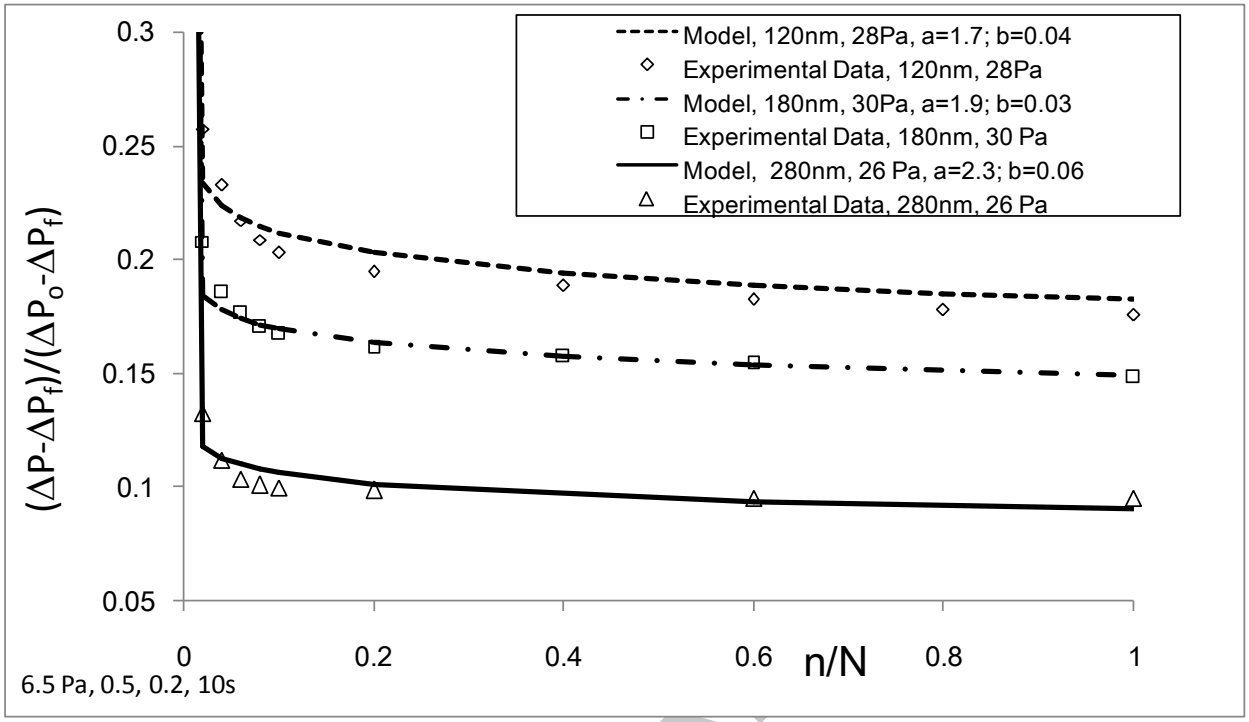

Fig. 8b - Close-up of pressure excursion across the filter during cleaning for the 3 filters with fiber diameter respectively 120, 180 and 280nm.

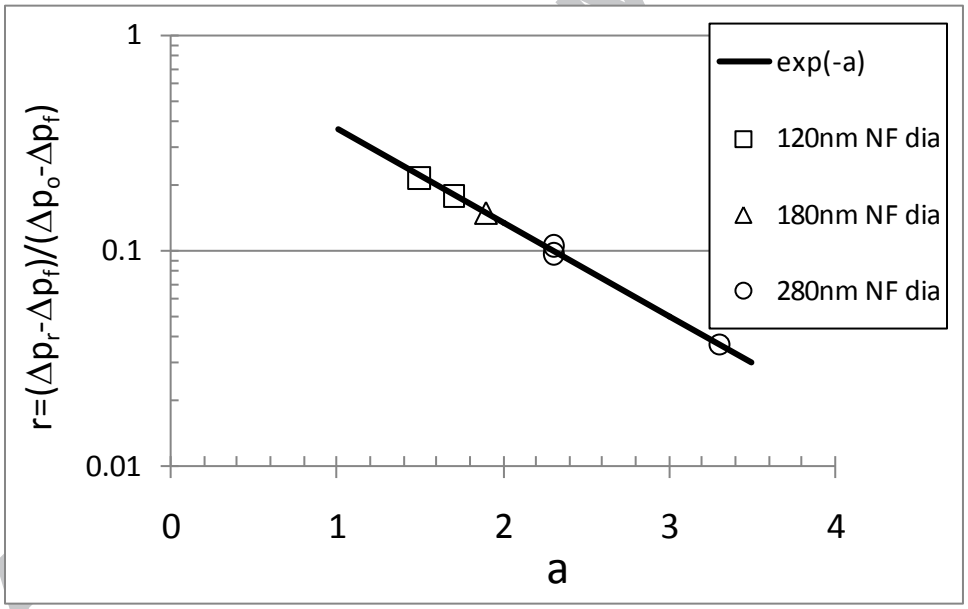

Fig. 8c - Residual ratio *r* plotted against *a* for the 3 filters with fiber diameters, respectively, 120, 180 and 280nm.

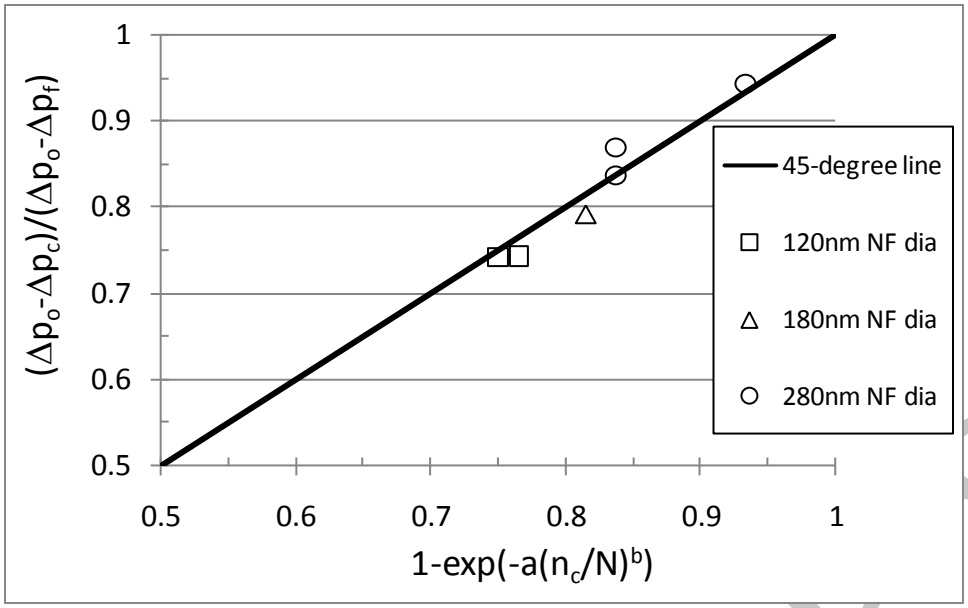

Fig. 8d - Cake discharge dimensionless ratio plotted against theoretical prediction for the 3 filters with fiber diameters, respectively, 120, 180 and 280nm.

4.5 Effect of various parameters on residual pressure

The effect on the residual ratio r from (i) backpulse, backblow, and combined back pulse and backblow; (ii) pulse durations; (iii) applied over pressure; (iv) fiber diameter of the filter; and (v) filter thickness effect are compiled in Fig. 9. As can be seen, regardless of the pros and cons that affect cleaning, they can be correlated by r=exp(-a) where a embodies all these factors. Higher *a* refers to better cleaning resulting in lower residual pressure *r* and lower aerosols in the filter, and vice versa. These effects can be combined to determine the appropriate *a* to achieve a certain residual level, which is very useful.

A general correlation of *a* with changing pulse, overpressure, fiber diameter and filter thickness as compared to the base-line level a_o can be in form of the following/

$$a = a_o\left(\frac{\Delta t_p}{\Delta t_{po}}\right)^{n_1}\left(\frac{\Delta p}{\Delta p_o}\right)^{n_2}\left(\frac{d_f}{d_{fo}}\right)^{n_3}\left(\frac{h}{h_o}\right)^{n_4} \qquad (11)$$

where a_o represents that of the base case (Δt_{po}, Δp_o, d_{fo}, h_o) and any deviation from the base case can be approximated by a power-law behavior with exponent "n_i" with i=1-4. For example, n_2=0.65 and Δp_o=6.5bar.

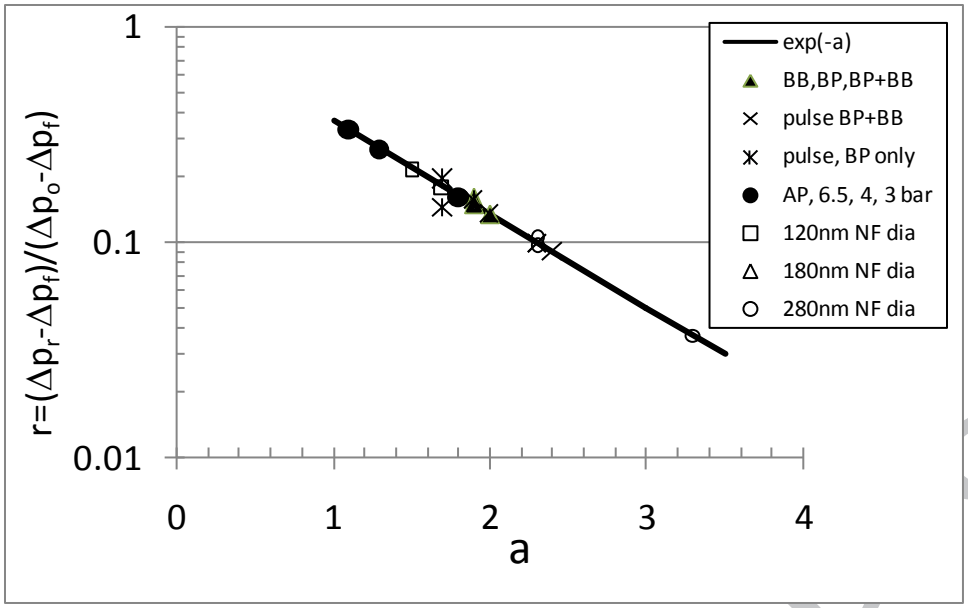

Fig. 9a - Residual pressure ratio for all tests

4.6 Effect of various parameters on cake discharge

The dimensionless cake pressure can be plotted against *b* as shown in Fig, 9b. There is in general a decrease of the dimensionless cake pressure with increasing *b* with the exception of the two outliers for 3 and 4 bar over-pressure (given by the solid circle symbols at bottom of the graph). The correlation is not very strong. This can be explained by the fact that the pressure drop is related to largely the cake removal and also to some extent the removal of some loosened aerosols in the nanofiber filter by the air jet. In other words, there will be some detachment of aerosols from the nanofibers inside the filter and possibly recapture by the filter downstream of the flow. Along this, the dimensionless cake pressure drop should also include not only parameter *b* but also parameter *a*. Therefore, it is indeed prudent to plot the dimensionless pressure drop against the driving force that involves both parameters *b* and *a*, $1-\exp(-a[n_c/N]^b$. Such plot is given in Fig. 9c. Notwithstanding the two outlier points, there is much better agreement between the dimensionless cake pressure drop, which reflects the fast dislodge of the cake plus some loose aerosols in the filter, and the driving force, $1-\exp(-a[n_c/N]^b$.

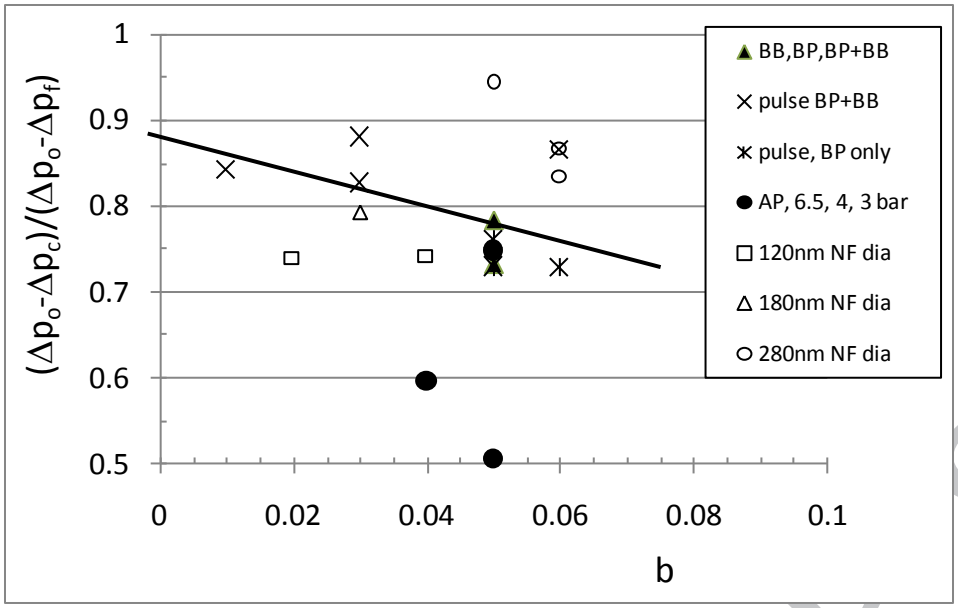

Fig. 9b - Cake discharge dimensionless ratio versus b

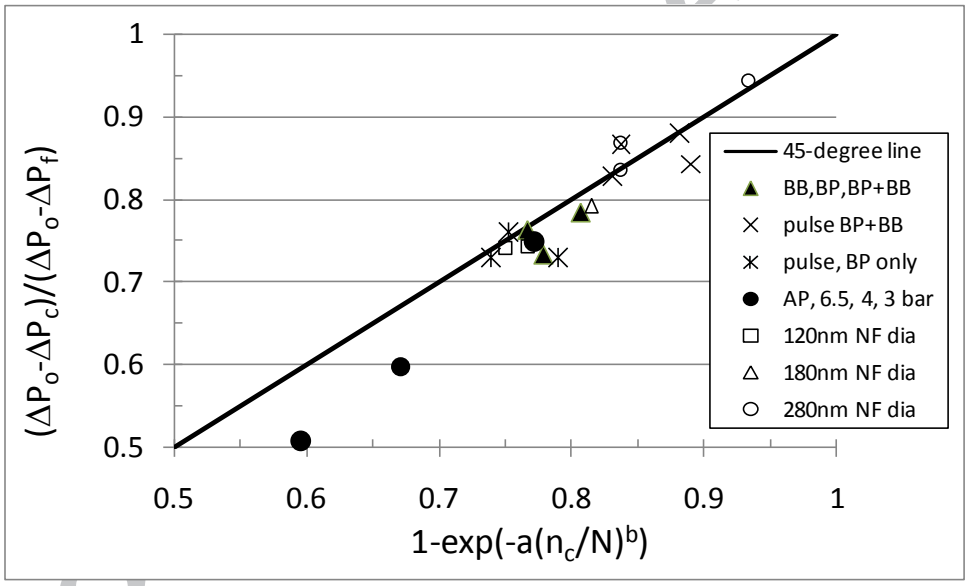

Fig. 9c - Cake discharge dimensionless ratio for all tests

5. CONCLUSIONS

A simple model has been developed empirically using two parameters *a* and *b*, where the dimensionless parameter *a* is related to detachment-to-attachment force and the recapture of the airborne aerosols which have been detached from the nanofibers. The dimensionless parameter *b* is related to cake discharge.

The fast drop in pressure due to cake discharge plus some loosened aerosols in the first stage and also the detachment and recapture of aerosols under equilibrium in the final or third stage have been accurately modeled. The transition which is the second stage can also be predicted reasonably well by this simple two-parameter model.

Five groups of parameters have been tested in the experiments conducted previously [1] and also in this work; and their results are reasonably well interpreted by the model. Three of these five groups concern how to effect a better “driving force to remove the trapped aerosols” in a loaded filter; namely, backpulse, backblow, and combined mode; pulse duration; and applied over-pressure. The other two groups of parameters address the “retention of the aerosols” such as increasing the adhesion by increasing the area of the fibers exposed to the aerosols simply by reducing the fiber diameter and increasing the filter thickness to recapture the aerosols. These parameters can be mixed and matched in various combinations to project the final residual solids as represented by the residual pressure in the filter. Also, combinations of operating parameters can be used to project the initial cake layer plus loosened aerosols being discharged (i.e. dimensionless cake pressure drop) from the filter at the initial cleaning stage.

6. ACKNOWLEDGEMENTS

The authors thank The Hong Kong Research Grant Council for supporting the project and supporting Curie WY Hau for two years of her studentship under Project B-Q33G.

7. REFERENCES

1. H.C. Lu, C.J. Tsai, "Numerical and experimental study of cleaning process of a pulse-jet fabric filtration system," *Environmental science & technology*, vol. 30, no. 11, pp. 3243-3249, 1996.

2. H.C. Lu, C.J. Tsai, "A pilot-scale study of the design and operation parameters of a pulse-jet baghouse," *Aerosol science and technology*, vol. 29, no. 6, pp. 510-524, 1998.

3. H.C. Lu, C.J. Tsai, "Influence of design and operation parameters on bag-cleaning performance of pulse-jet baghouse," *Journal of Environmental Engineering*, vol. 125, no. 6, pp. 583-591, 1999.

4. S. LAUX, U. RENZ, "Pressure cleaning of ceramic filter elements for the hot gas filtration," *Dissertation RWTH Aachen*, 1993.

5. R. Mai, M. Fronhöfer, H. Leibold, "Flow characteristics of filter candles during recleaning," *High Temperature Gas Cleaning*, pp. 194-206, 1996.

6. W. Humphries, J.J. Madden, "Fabric filtration for coal-fired boilers: dust dislodgement in pulse jet filters," *Filtration and Separation*, vol. 20, no. 1, pp. 40-44, 1983.

7. S.K. Grannell, J.P.K. Seville, "Effect of venture inserts on pulse cleaning of rigid ceramic filters," *High Temperature Gas Cleaning*, vol. 2, pp. 96-110, 1999.

8. J.H. Choi, Y.G. Seo, J.W. Chung, "Experimental study on the nozzle effect of the pulse cleaning for the ceramic filter candle," *Powder Technology*, vol. 114, no. 1-3, pp. 129-135, 2001.

9. L.M. Lo, D.R. Chen, D.Y.H. Pui, "Experimental study of pleated fabric cartridges in a pulse-jet cleaned dust collector," *Powder Technology*, vol. 197, no. 3, pp. 141-149, 2010.

10. M. De Ravin, W. Humphries, R. Postle, "A model for the performance of a pulse jet filter," *Filtration and Separation*, vol. 25, no. 3, pp. 201-207, 1988.

11. J. Sievert, F. Löffler, "Fabric cleaning in pulse-jet filters," *Chemical Engineering and Processing: Process Intensification*, vol. 26, no. 2, p. 179–183, 1989.

12. P. Geang, Update of VDI-Guideleine 3926 "Testing of Filter Media for Cleanable Filters" and Development of a Mobile Filter Probe for Field Measurements", 6th Symposium "Textile Filters", March 5th and 6th 2002, Chemnitz, Germany.

13. C.W.Y. Hau, W.W.F. Leung, "Experimental Investigation of Backpulse and Backblow Cleaning of Nanofiber Filter loaded with Nano-aerosols", dx.doi.org/10.1016/j.seppur.2016.02.041.